Open access • Proceedings Article • DOI:10.2514/6.2015-2210

Large-eddy simulation of underexpanded round jets impinging on a flat plate 4 to 9 radii downstream from the nozzle — Source link

Romain Gojon, Christophe Bogey, Olivier Marsden

Institutions: École centrale de Lyon

Published on: 22 Jun 2015 - AIAA/CEAS Aeroacoustics Conference

Topics: Jet (fluid), Stagnation pressure, Nozzle, Mach number and Reynolds number

Large-eddy simulation of underexpanded round jets impinging on a flat plate 4 to 9 radii downstream from the nozzle

Romain Gojon*, Christophe Bogey† and Olivier Marsden‡

Laboratoire de Mécanique des Fluides et d'Acoustique

UMR CNRS 5506, Ecole Centrale de Lyon

69134 Ecully, France

Supersonic round jets have been computed by compressible Large Eddy Simulation (LES) using low-dispersion and low-dissipation schemes. The jets are underexpanded, and are characterized by a Nozzle Pressure Ratio of $NPR = P_r/P_{amb} = 4.03$, where P_r is the stagnation pressure and P_{amb} is the ambient pressure. They have a fully expanded Mach number of $\mathcal{M}_j = 1.56$, an exit Mach number of $\mathcal{M}_e = 1$, and a Reynolds number of $Re_j = u_j D/\nu = 5 \times 10^4$, where u_j and D are the jet fully expanded exit velocity and the nozzle diameter, respectively. A free jet is first considered. Four jets impinging on a flat plate normally are then examined. The distance L between the nozzle lip and the flat plate varies from $L = 4.16r_0$ up to $L = 9.32r_0$ where $r_0 = D/2$, for the impinging jets. The effects of the plate on the aerodynamic and acoustic properties of the jets are thus studied. For the free jet, snapshots of density, pressure and vorticity are presented. Mean velocity fields are displayed, they are in good agreement with experimental data. The near pressure field of the jet is investigated using Fourier decomposition. A screech tone component is found, at a frequency comparing well with experimental data and theoretical models. For the four impinging jets, similarly, flow snapshots and mean flow fields are shown. The results obtained are similar to the corresponding measurements. The convection velocity of large-scale structures in the jet shear layers is then evaluated and an expression giving the average convection velocity between the nozzle lips and the flat plate is proposed. The near pressure fields are then explored, and the main properties of the aeroacoustic feedback mechanism occurring between the nozzle lip and the flat plate are presented. The results are consistent with theoretical models and experimental data.

I. Introduction

Very intense tones were observed experimentally by Powell[1] and Wagner,[2] among others, in the acoustic field of high subsonic and supersonic jets impinging on a flat plate normally. Moreover, as the distance between the nozzle and the flat plate varies, a staging phenomenon of the main tone frequency was obtained. Powell[1] suggested that such tones are generated by a feedback mechanism between hydrodynamic instabilities propagating downstream from the nozzle to the plate and acoustic waves propagating upstream from the plate to the nozzle.

For round subsonic impinging jets, Ho & Nosseir[3] and Nosseir & Ho[4] built a model to predict the tone frequencies of the feedback mechanism. This model is based on cross-correlations between microphones in the near field of impinging jets. Later, Tam & Ahuja[5] proposed that the upstream-propagating waves of the feedback mechanism correspond to neutral acoustic wave modes of the jets. They found an allowable frequency range for each upstream propagating neutral acoustic wave mode of the jet flow using a vortex sheet jet model. They obtained results in line with the experimental data of Wagner[2] for high subsonic round jets. Round supersonic jets impinging on a flat plate normally have been investigated experimentally by Henderson

*PhD, romain.gojon@ec-lyon.fr.

†CNRS Research Scientist, AIAA Senior Member & Associate Fellow, christophe.bogey@ec-lyon.fr.

‡olivier.marsden@ec-lyon.fr.

& Powell,[6] Krothapalli *et al.*[7] and Henderson *et al.*[8] In some cases, a feedback mechanism is observed as in subsonic jets. This is very often the case when the jet is ideally expanded, but only for some nozzle-to-plate distances when the jet is imperfectly expanded. Henderson & Powell[6] suggested that, in the latter case, the feedback establishes only when a Mach disk forms upstream from the plate. Recirculation zones were also observed near the flat plate by Krothapalli *et al.*[7] More recently, for underexpanded impinging jets, Risbord & Soria[9] explored the instability modes of the jets using ultra-high-speed Schlieren and shadowgraphy techniques. Axial and helical modes have been identified and the Mach disk located upstream from the plate has been observed to oscillate. For similar jets, Buchmann *et al.*[10] observed the periodic formation of large-scale structures in the jet shear layers using a high spatial resolution Schlieren imaging. The complete feedback mechanism is visible, and includes large-scale structures in the shear layers propagating downstream from the nozzle to the plate and acoustic waves propagating upstream from the plate to the nozzle. Finally, Mitchell *et al.*[11] studied the periodic oscillation of the shear layer of underexpanded impinging jets using time-resolved Schlieren image sequences. Unfortunately, the connections between the different flow features listed above, namely, the shock-wave oscillations, the periodic shear-layer instabilities, the recirculation zones near the plate, and the production of tones, remain unclear. In order to understand these interactions, Kuo & Dowling[12] considered that there is a flux resonance in the region of impact between the Mach disk and the flat plate, and they developed a 1-D model of the Mach disk motion involving acoustic and entropy waves. With this model, a resonance condition is found, and for a given mean velocity flow, the frequency of resonance of the Mach disk motion can be estimated. The predicted resonance frequencies matched the experimental tone frequencies observed by Powell[13] only for small plates, although the model was supposed to be adapted to all plate sizes. Moreover, the model is only valid when there is no recirculation zones between the Mach disk and the plate. When the jet is strongly underexpanded and the plate is located in the first cell of the free equivalent jet, a feedback loop involving disturbances in the shear layer between the subsonic region downstream of the Mach disk and the supersonic peripheral flow was proposed by Henderson *et al.*[8] Numerical simulations were conducted by Dauptain *et al.*[14,15] for such configurations, and a modified model to predict the tone frequencies of the feedback loop was proposed.

In the present work, the LES of five round jets are carried out in order to investigate the feedback mechanism occurring between the nozzle lip and the flat plate for impinging jets. In particular, the spectral and hydrodynamic properties of the jets are studied and compared with experimental data and theoretical models. The paper is organized as follows. The jets parameters and the numerical methods used for the LES are given in section II. The aeroacoustic properties of the free jet is then presented in section III, and compared with experimental data and theoretical models. The four jets impinging on a flat plate are then described in section IV, and the feedback mechanism is studied by evaluating the convection velocity and describing the near pressure fields of the jets. Concluding remarks are given in section V.

II. Parameters

II.A. Jets parameters

Large-eddy simulations are performed for four jets impinging on a flat plate with nozzle-to-plate distances L/r_0 of 4.16, 5.6, 7.3 and 9.32, and for a free jet, as shown in table 1. The jets are referred to as JetL4, JetL5, JetL7 JetL9, and Jetfree, respectively. The ejection conditions of the jets and the nozzle-to-plate distances are similar to the conditions in the experiments of Henderson *et al.*[8] The jets have a Nozzle Pressure Ratio of $NPR = P_r/P_{amb} = 4.03$, a fully expanded Mach number of $\mathcal{M}_j = 1.56$, a Reynolds number of $Re_j = u_j D/\nu = 5 \times 10^4$ and an exit Mach number of $\mathcal{M}_e = 1$. They originate from a pipe nozzle whose lip thickness is equal to $0.1r_0$. At the nozzle exit, a Blasius boundary-layer mean velocity profile is imposed with a boundary-layer thickness of $\delta_{BL} = 0.15r_0$.

II.B. Numerical parameters

The unsteady compressible Navier-Stokes equations are solved on a cylindrical mesh (r, θ, z) by using an explicit six-stage Runge-Kutta algorithm for time integration, and low-dispersion and low-dissipation explicit eleven-point finite differences for spatial derivation.[16,17] At the end of each time step, a relaxation filtering is applied to the flow variables in order to remove grid-to-grid oscillations and to dissipate subgrid-scale turbulent energy.[18,19] The radiation conditions of Tam & Dong[20] are implemented at the inflow and lateral boundaries of the computational domain. A sponge zone combining grid stretching and Laplacian filtering

	$\mathcal{M}_j$	Re_j	L/r_0
JetL4	1.56	5×10^4	4.16
JetL5	1.56	5×10^4	5.6
JetL7	1.56	5×10^4	7.3
JetL9	1.56	5×10^4	9.32
Jetfree	1.56	5×10^4	-

Table 1. Jet parameters: fully expanded Mach number $\mathcal{M}_j$, Reynolds number Re_j, and nozzle-to-plate distance L/r_0.

is also employed to damp the turbulent fluctuations before they reach the lateral boundaries. The present solver has been previously used[21,22] to simulate 3-D round jets at a Mach number $\mathcal{M}_e = 0.9$. Adiabatic conditions are imposed to the nozzle walls and to the flat plate. A shock-capturing filtering is applied in order to avoid Gibbs oscillations near shocks. It consists in applying a conservative second-order filter optimised in Fourier space at a magnitude determined each time step using a shock sensor.[23] This method was successfully used by de Cacqueray *et al.*[24] for the LES of an overexpanded jet at Mach number $\mathcal{M}_e = 3.3$. Moreover, low-amplitude vortical disturbances, not correlated in the spanwise direction,[21] are added in the boundary layer in the nozzle, at around $z = -r_0$ and $r = 0.90r_0$, in order to generate velocity fluctuations at the nozzle exit. The strength α of the forcing is fixed to 0.02 to obtain turbulent intensities between 5% and 10% of the fully expanded jet velocity at the nozzle exit. This value is similar to those used in Bogey *et al.*[21] The axis singularity is treated with the method proposed by Mohseni & Colonius.[25] Notably, the first point close to the axis is located at $r = \Delta r/2$, where Δr is the radial mesh size. Finally, a reduction of the effective resolution near the origin of the polar coordinates is implemented,[26] in order to increase the admissible time step of the simulation.

	n_r	n_θ	n_z	number of points
JetL4	500	512	668	171×10^6
JetL5	500	512	764	195×10^6
JetL7	500	512	780	200×10^6
JetL9	500	512	847	217×10^6
Jetfree	500	512	1561	400×10^6

Table 2. Mesh parameters: number of points in the radial, azimuthal and axial direction, and total number of points.

The simulations are carried out using an OpenMP-based in-house solver, and a total of 180,000 iterations are computed in each case for the steady state. The simulation time is thus equal to $1000r_0/u_j$. The cylindrical meshes (n_r, n_θ, n_z) contain between 171 and 400 million points, as reported in table 2. The variations of the radial and axial mesh spacings are represented in figure 1.

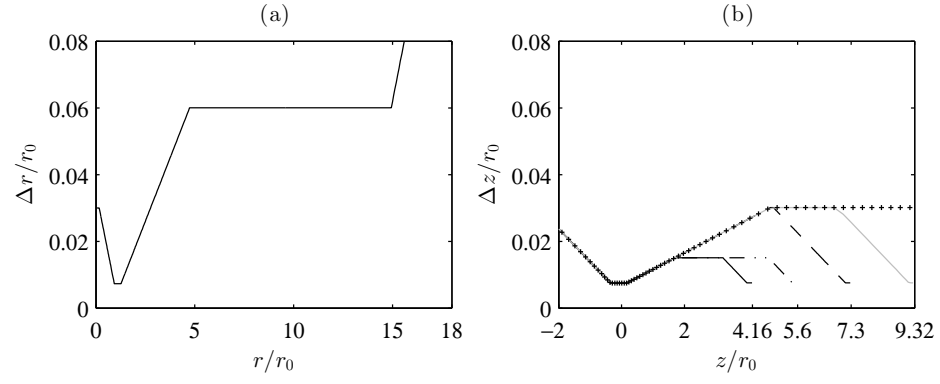

Figure 1. Representation of: (a) radial mesh spacings, and (b) axial mesh spacings: —— JetL4, —·— JetL5, — — — JetL7, —— JetL9 and + + + Jetfree.

For the impinging jets, the minimal axial mesh spacing, near the nozzle lip and the flat plate, is equal to $\Delta z = 0.0075r_0$, and the maximal axial mesh spacing, between the nozzle and the plate, is equal to

$\Delta z = 0.015 r_0$ for JetL4 and JetL5, and to $\Delta z = 0.03 r_0$ for JetL7 and JetL9. The minimal radial spacing is $\Delta r = 0.0075 r_0$ at $r = r_0$, and the maximal radial spacing is $\Delta r = 0.06 r_0$ for $5r_0 \leq r \leq 15r_0$. Then, for $r \geq 15r_0$, a sponge zone is implemented. For the free jet, the grid is the same in the radial direction, but differs in the axial direction far from the nozzle with a maximal axial mesh spacing of $\Delta z = 0.03 r_0$ for $5r_0 \leq z \leq 30r_0$, and a sponge zone for $z \geq 30r_0$. These discretizations allow acoustic waves with Strouhal numbers up to $St_D = fD/u_e = 6.4$ to be well propagated, where f is the frequency. Finally, note that grids are stretched at rates lower than 1% outside the sponge zones, in order to preserve numerical accuracy.

III. Results for the free jet

The results obtained for the free jet are first described for validation of the numerical set-up and for comparison with the results for the impinging jets.

III.A. Flow snapshots

In order to illustrate the shear-layer development downstream of the nozzle, a snapshot of the vorticity norm obtained in the plane (z, r) is presented in figure 2. The shear layer develops rapidly downstream of the nozzle exit with both small and large turbulent structures, in agreement with the Reynolds number of $Re_j = 5 \times 10^4$. The end of the jet potential core appears to be located around $17.5 r_0$. Lau *et al.*[27] proposed an empirical model for the length of the potential core z_p for isothermal jets with Mach number up to 2.5, which writes

$$\frac{z_p}{D_j} = 4.2 + 1.1 \mathcal{M}_j^2 \tag{1}$$

where D_j and $\mathcal{M}_j$ are the fully expanded diameter and the Mach number of the jet.

For the present free jet, the parameters $\mathcal{M}_j = 1.56$ and $D_j = 2.2$mm give a potential core length of $z_p = 15 r_0$. Tam *et al.*[28] included in the expression (1) the temperature ratio between the stagnation and the ambient temperatures in order to take into account compressibility effects. This expression gives $z_p = 17.5 r_0$. A good overall agreement is thus found between the present result and the empirical expression derived by Tam *et al.*[28]

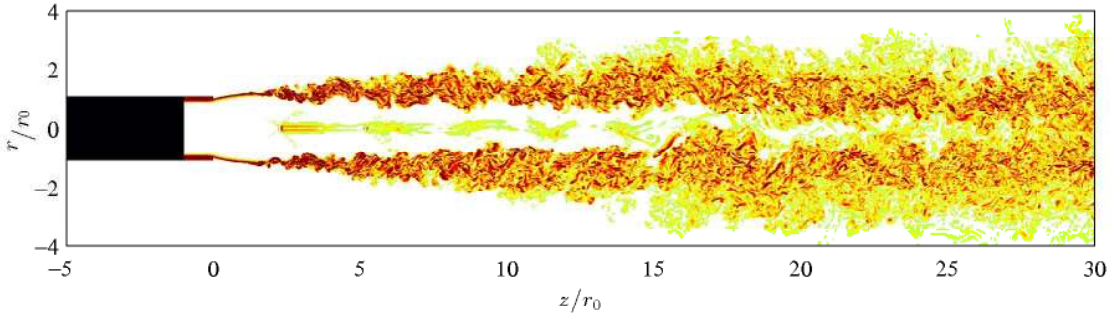

Figure 2. Snapshot in the (z, r) plane of the vorticity norm $|\omega|$ for Jetfree. The colour scale ranges up to the level of $10 u_e/D$.

In order to visualize both the flow and acoustic fields, a snapshot in the (z, r) plane of the density and the fluctuating pressure is provided in figure 3(a). A shock-cell structure, typical of an underexpanded jet, is obtained with around ten shock cells visible. Because the jet is highly underexpanded, a Mach disk is found in the first cell, at $z = 2.35 r_0$ and shear layers can be observed in figure 2 between the subsonic and the supersonic region downstream of the Mach disk. This is in agreement with the results of Powell,[13] Henderson,[29] and Addy,[30] who noted that a Mach disk is generated in underexpanded jets for $NPR > 3.8$ or 3.9. In the pressure field, acoustic waves and two acoustic contributions can be seen. First, circular wavefronts are visible and seem to originate from the first five cells. They are due to the interactions between the shocks and the turbulence in the jet shear layers. Upstream propagating acoustic waves can also be observed on each side of the jet, in the vicinity of the nozzle. For the comparison, a *Schlieren* picture of an underexpanded jet obtained by André *et al.*[31] is displayed in figure 3(b). The fully expanded Mach number of the jet is $\mathcal{M}_j = 1.55$ and the exit Mach number is $\mathcal{M}_e = 1$. A great similarity is noted with

the computed jet. In particular, the Mach disk is clearly visible in the first cell as well as the shear layers downstream.

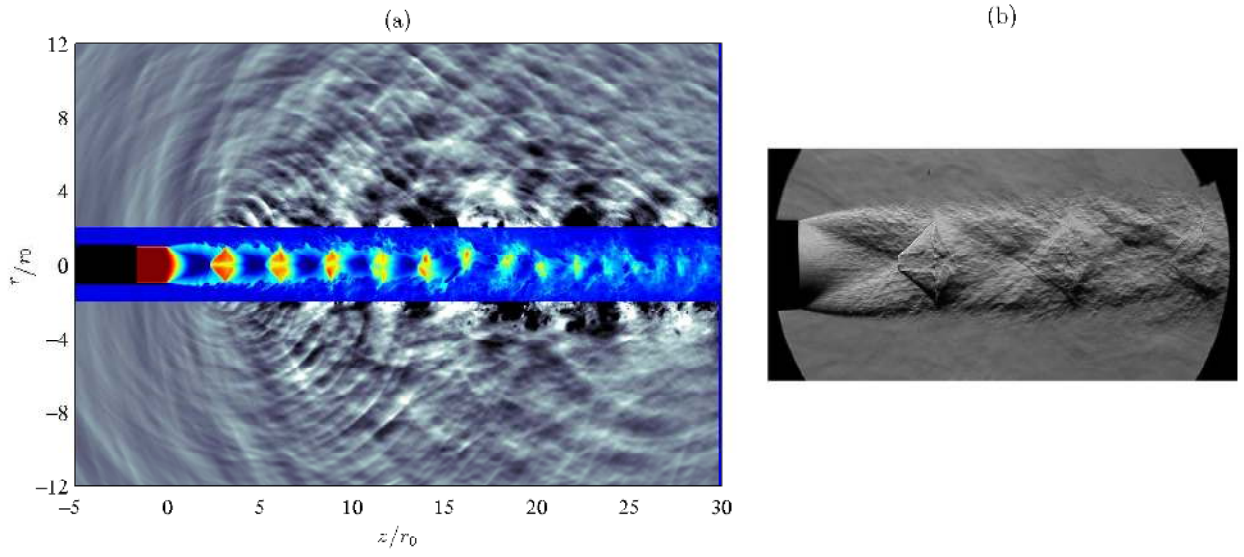

Figure 3. (a) Snapshot in the (z, r) plane of the density in the jet and close to the flat plate, and of the fluctuating pressure for Jetfree. The colour scale ranges from 1 to 3 kg.m^{-3} for the density and from −2000 to 2000 Pa for the pressure; (b) Schlieren picture of an underexpanded jet obtained by André *et al.*[31] for a $\mathcal{M}_j = 1.55$ and $\mathcal{M}_e = 1$ jet.

III.B. Mean fields

The mean axial and radial velocity fields are presented in figure 4, where the experimental PIV results of André *et al.*[31] are also displayed. The geometry of the shock-cell structure and the levels obtained in the LES and in the experiment are in good agreement.

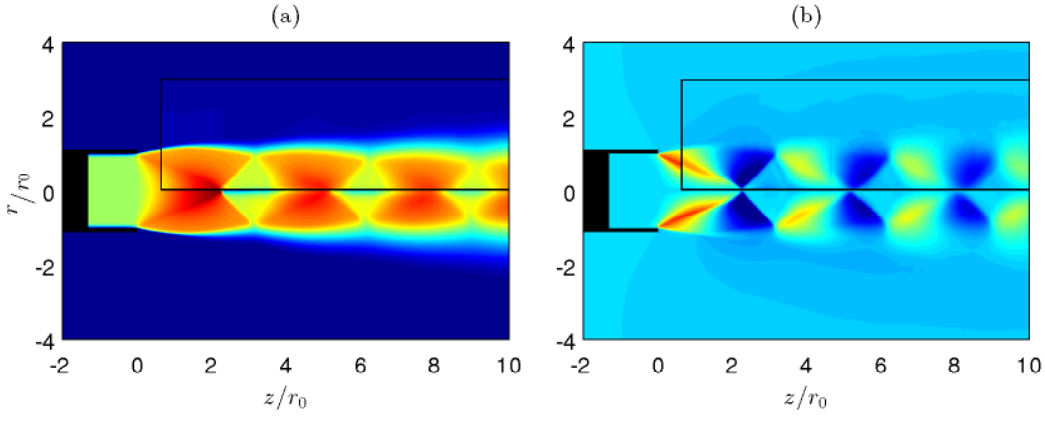

Figure 4. Mean fields in the (z, r) plane of (a) axial and (b) radial velocities for Jetfree. The colour scale ranges from 0 to 600 m.s^{-1} for the axial velocity and from −150 to 150 m.s^{-1} for the radial velocity; the PIV results of André *et al.*[31] for a $\mathcal{M}_j = 1.55$ and $\mathcal{M}_e = 1$ jet are displayed in the black rectangles.

In figure 4(a), the length of the first shock cell L_s of the jet appears to be $3.20r_0$. This result is identical to those of Henderson *et al.*[8] for a similar free jet. Besides, the length of the first cell can be estimated by using a first-order shock solution based on the pressure ratio p_s/p_a, where p_s is the pressure perturbation of the shock-cell structure and $p_s + p_a$ is the actual pressure in the jet. This solution was first proposed by Prandtl[32] in 1904. Later, the following approximated solution was given by Tam & Tanna:[33]

$$L_s = \frac{\pi D_j \beta}{\mu_1} \simeq 1.306 \beta D_j \tag{2}$$

where μ_1 is the first zero of the zero-order Bessel functions of the first kind and $\beta = \sqrt{\mathcal{M}_j^2 - 1}$. This expression is called Prandt formula. Expression (2), for the present jet, provides $L_s = 3.45r_0$, which is slightly larger than the measured and computed values. Later, the expression (2) was improved by Pack[34] by calculating the first forty coefficients of the model of Prandtl,[32] yielding $L_s = 1.22\beta D_j$, hence $L_s = 3.20r_0$ for the present jet, which is similar to the values reported above.

The shock-cell size seems to decrease with the downstream distance in figure 4(a). This evolution is due to the growth of the shear layer and to the dissipation of the shock-cell structure. The decrease of the normalized shock-cell size is presented in figure 5 for the present jet and for the jets of André *et al.*[31] A good agreement is found between the present jet and the experimental results.[31] A linear variation of the shock-cell size is also obtained, as observed by Harper-Bourne & Fisher[35] for instance.

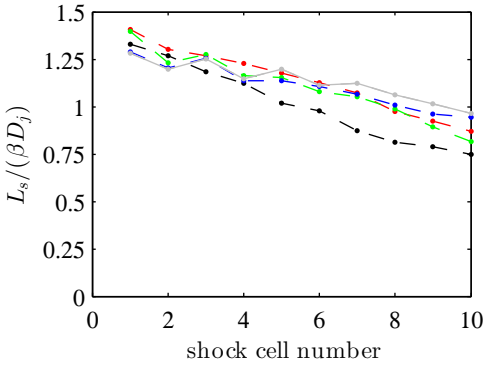

Figure 5. Normalized lengths of the first ten shock cells in − • − the present jet, and the experimental jets of André *et al.*[31] with − • − $\mathcal{M}_j = 1.50$, − • − $\mathcal{M}_j = 1.35$, − • − $\mathcal{M}_j = 1.15$ and − • − $\mathcal{M}_j = 1.10$.

For the first eight cells of the present jet, the mean velocity field provides a total size of $20.5r_0$. For underexpanded supersonic jets, Harper-Bourne & Fisher[35] and Seiner & Norum[36] obtained an empirical expression for the size of the first eight cells, which writes $L_t = 1.11\beta D$. For the present jet, the formula provides $L_t = 21.5r_0$, which is consistent with the above value.

Finally, the Mach disk located at $z_M = 2.3r_0$ is a normal shock wave. For a normal shock, the Rankine-Hugoniot jump condition leads

$$\frac{u_2}{u_1} = \frac{(\gamma - 1)\mathcal{M}_1^2 + 2}{(\gamma + 1)\mathcal{M}_1^2} \tag{3}$$

where u_1 and u_2 are the velocities upstream and downstream of the normal shock wave respectively, and $\mathcal{M}_1$ is the upstream Mach number. In the present jet, one sets $u_1 = 595$ m.s^{-1} and $\mathcal{M}_1 = 2.75$ before the Mach disk and $u_2 = 166$ m.s^{-1} after the Mach disk. The latter value compares very well with the value $u_{2_{RH}} = 164$ m.s^{-1} predicted by the Rankine-Hugoniot jump condition. The Mach disk position z_M and diameter D_M can also be estimated from the mean velocity field, yielding $z_M = 2.3r_0$ and $D_M = 0.25r_0$. Experimentally, Addy[30] observed a Mach disk for jets with a NPR exceeding 3.9, and obtained the following empirical expressions:

$$\frac{z_M}{D_j} = 0.65\sqrt{NPR} \tag{4}$$

$$\frac{D_M}{D_j} = 0.36\sqrt{NPR} - 3.9 \tag{5}$$

The Mach disk positions and diameters obtained from the present simulation, the experiments of Addy[30] and expressions (4) and (5), are plotted as a function of the Nozzle Pressure Ratio in figure 6. A good overall agreement is found. It can be noted that expression (4) slightly overestimates the position of the Mach disk for $NPR < 6$.

III.C. Acoustic results

The sound pressure level (SPL) obtained near the nozzle exit at $z = 0$ and $r = 2r_0$ is displayed in figure 7 as a function of the Strouhal number $St_D = fD/u_e$. One tone emerges 15 dB above the broadband noise at

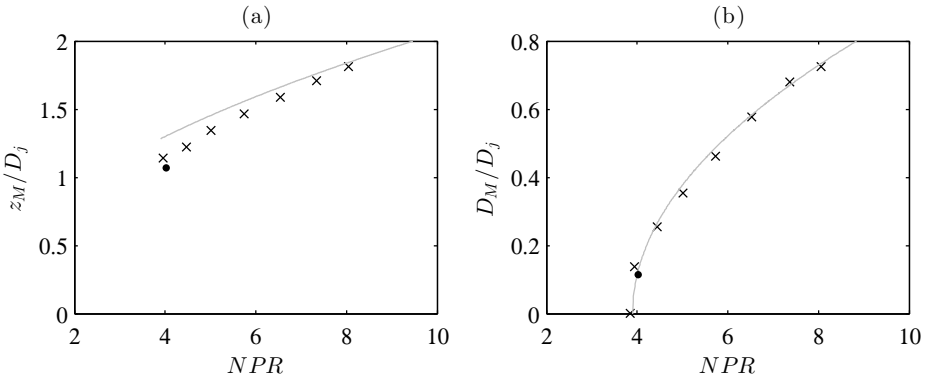

Figure 6. (a) Position and (d) diameter of the Mach disk at the end of the first shock cell obtained: • for Jetfree, × in the experiment of Addy[30] and —— using expressions (4) and (5).

a Strouhal number of $St_D = 0.38$. Such a result is typical of a screeching jet, see for instance in Westley & Woolley,[37] Tam & Tanna,[33] Panda,[38] and André *et al.*[31] The tone at $St_D = 0.38$ can therefore be attributed to the generation of screech noise by the jet.

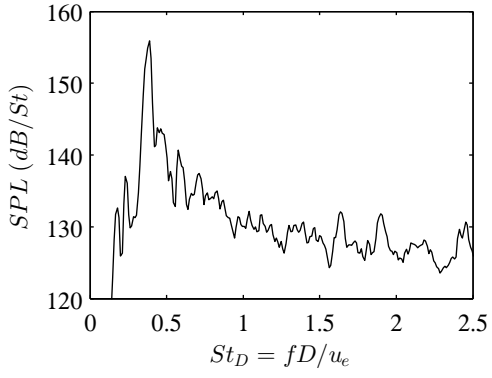

Figure 7. Sound pressure level (SPL) at $r = 2r_0$ and $z = 0$ as a function of the Strouhal number for Jetfree.

The near pressure fields in the (z, r) plane have been recorded every 50^{th} time step. The results are arranged in the $M \times N$ matrix:

$$P_{all} = \begin{bmatrix} P_1^1 & P_1^2 & . & P_1^N \\ P_2^1 & P_2^2 & . & P_2^N \\ . & . & . & . \\ P_M^1 & P_M^2 & . & P_M^N \end{bmatrix} \tag{6}$$

where N is the number of samplings, and $M = n_z \times 2n_r$ is the total number of points in a (z, r) plane. The pressure field obtained at a given time is thus provided by one column of P_{all}. A Fast Fourier Transform is applied to each row of the matrix P_{all}. In this way, for a given frequency, the amplitude and the phase fields can be displayed. For the tone at $St_D = 0.38$, they are given in figure 8. The amplitude field in figure 8(a) exhibits a cell structure different from the shock-cell structure. Such a structure is observed in the presence of an hydrodynamic-acoustic standing wave, as is the case in supersonic screeching jets, see in Panda.[38] The typical cell length in this structure is equal to the wavelength L_{sw} of the standing wave formed between the downstream propagating large-scale structures in the shear layers and the upstream propagating acoustic waves. The screech frequency f_s associated with this wavelength is provided by the model of Panda:[38]

$$f_s = \frac{u_c}{L_{sw}(1 + u_c/c_0)} \tag{7}$$

where u_c is the mean convection velocity of the structures in the shear layers and c_0 is the ambient sound speed. For the present jet, the cell structure in figure 8(a) shows a spatial periodicity of $L_{sw} \simeq 2.5r_0$. The

mean convection velocity, computed from cross-correlations of axial velocity fluctuations in the shear layers, see in section IV, is $u_c = 0.65u_j$, where u_j is the fully expanded jet velocity. Expression (7) thus leads to a screech Strouhal number of $St_D = f_s D/u_e \simeq 0.38$, which is in agreement with the tone frequency of figure 7.

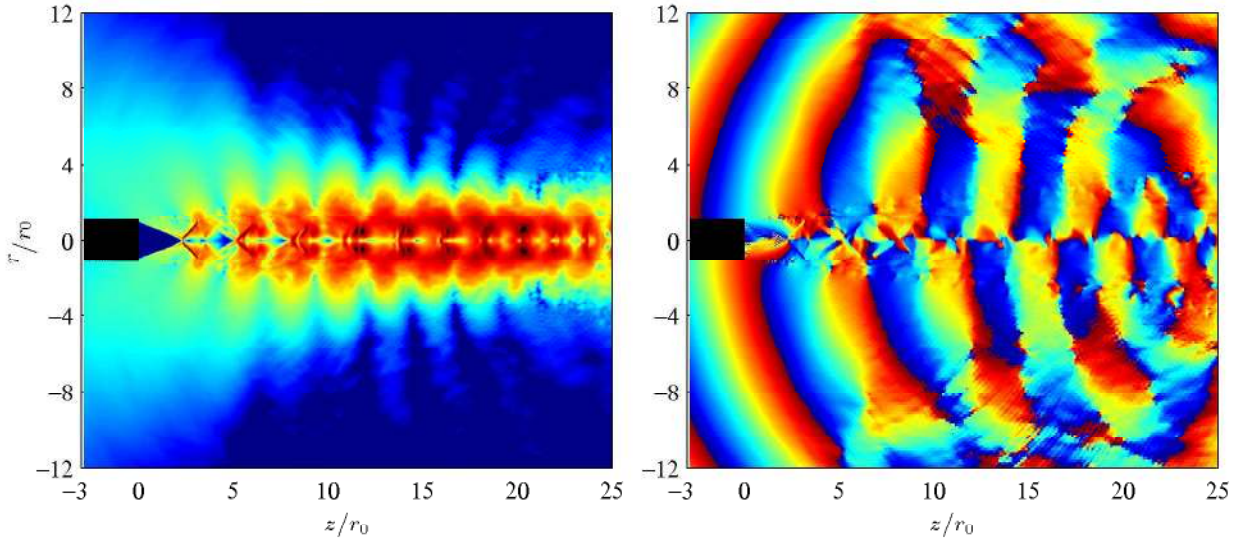

Figure 8. Amplitude (a) and phase (b) fields in the (z, r) plane obtained for the dominant tone frequency of Jetfree at $St_D = 0.38$.

In figure 8(b), a 180 degree phase shift with respect to the jet axis is visible. This indicates that the mode at $St_D = 0.38$ is sinuous or helical. More precisely, using a Fourier decomposition of the fluctuating pressure on 32 sensors regularly-spaced in the azimuthal direction, at $z = 0$ and $r = 2r_0$, it turns out to be helical. This mode is compared in figure 9 with the dominant screech tones found in the experiments of Powell *et al.*[39] for round supersonic underexpanded jets. These tones are associated with varicose modes ($A1$ and $A2$), with sinuous and sometimes helical modes (B), with helical modes (C), and with sinuous modes (D). The screech tone in the present jet falls in the vicinity of tones C, in agreement with the results reported above. Consequently, both the frequency and the nature of the screech mode in Jetfree are consistent with the theoretical predictions of Panda[38] and the measurements of Powell *et al.*[39]

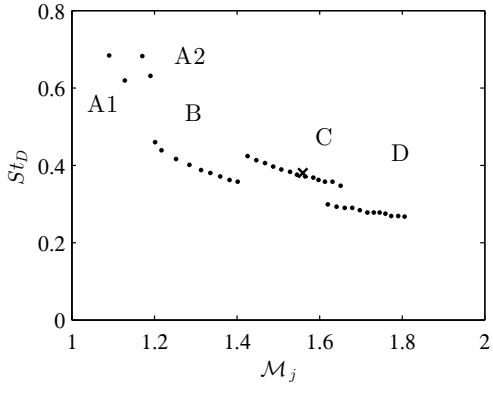

Figure 9. • Dominant screech tone frequencies obtained in the experiments of Powell *et al.*[39] as a function of the fully expanded Mach number $\mathcal{M}_j$; × dominant screech tone frequency in Jetfree.

In the next section, jets with the same exit conditions as Jetfree impinging normally on a flat plate for four different nozzle-to-plate distances are presented. The positions of the plate with respect to the shock-cell structure of Jetfree are shown in figure 10. For JetL4, with $L = 4.16r_0$, the plate is located in the first half of the second cell of the shock-cell structure, where the velocity increases and the pressure decreases with the axial distance on the jet centerline, whereas for JetL5, with $L = 5.6r_0$, it lies in the second half of the second cell, where velocity decreases and pressure increases. For JetL7 and JetL9, with $L = 7.3r_0$ and $L = 9.32r_0$, the plates are located in the first halves of the third and of the fourth cells of the shock-cell structure,

respectively. These remarks are of interest, given that, according to Henderson *et al.*,[8] the occurrence of intense tones in imperfectly expanded impinging jets depends on the location of the plate in the shock-cell structure of the corresponding free jet.

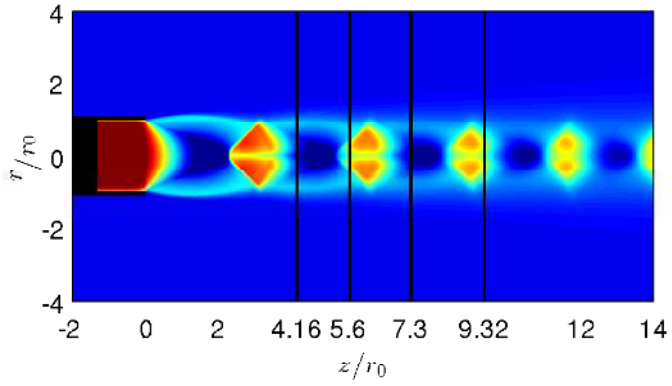

Figure 10. Mean density field in the (z, r) plane for Jetfree. The colour scale ranges from 1 to 3 kg.m^{-3}. The black lines correspond to the position of the plates for the impinging jets.

IV. Results for the impinging jets

IV.A. Flow snapshots

In order to illustrate the flow fields in the impinging jets, isosurfaces of density are displayed in figure 11 for JetL9. In the jet, a shock-cell structure appears clearly between the nozzle and the plate in blue an red. The boundaries of the mixing layers are also well visible in cyan. In addition, longitudinal structures can be seen on the outer border of the first shock cell. They have been described in different experiments, including those by Arnette *et al.*[40] They are due to small perturbations at the nozzle exit, which are amplified by Taylor-Goertler-type instabilities, and are specific to underexpanded jets.

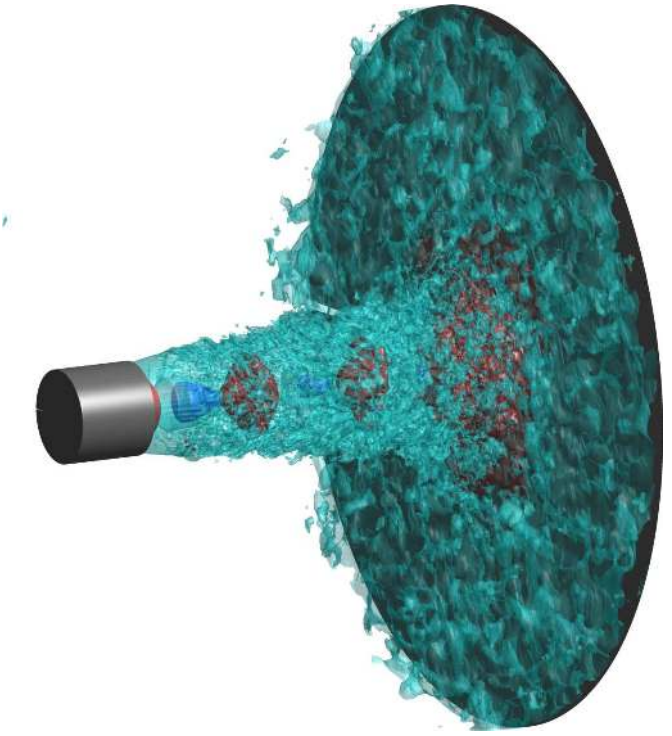

Figure 11. Isosurfaces of density for JetL9. The blue, cyan and red isosurfaces correspond to the values of 0.8, 1.25 and 2.5 kg.m^{-3}, respectively. The nozzle and the flat plate are represented in grey.

Snapshots of the vorticity norm obtained in the (z, r) plane for JetL4, JetL5, JetL7 and JetL9, are presented in figure 12. In JetL4, in figure 12(a), large vortical structures of typical size $0.2r_0$ are found in the shear layers. They are strongly correlated in the azimuthal direction (not shown here). The distance between the two sliplines visible downstream of the Mach disk at $z \simeq 2r_0$, equal to $0.5r_0$, is larger than that in the free jet, equal to $0.23r_0$, which results from a larger diameter of the Mach disk. In JetL5, JetL7 and JetL9, the shear layers develop in the same way as in Jetfree with both small and large turbulent structures. The distance between the sliplines downstream of the Mach disk is also the same as in Jetfree.

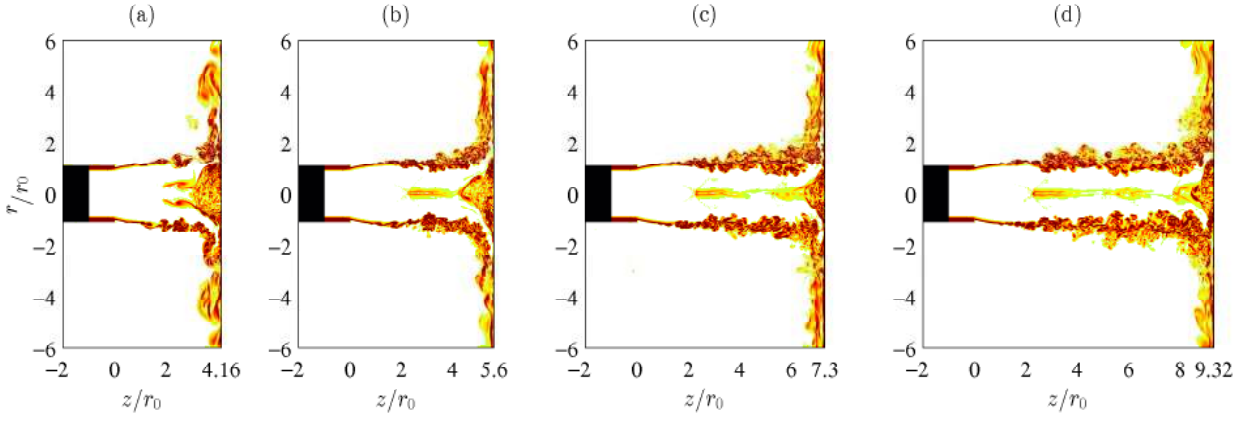

Figure 12. Snapshots in the (z, r) plane of the vorticity norm $|\omega|$ for for (a) JetL4, (b) JetL5, (c) JetL7 and (d) JetL9. The colour scale ranges up to the level of $10u_e/D$.

Snapshots of density and fluctuating pressure in the (z, r) plane are provided in figure 13 for the four jets. In figure 13(a), for JetL4, one shock cell appears in the density field. Compared to the free jet where the Mach disk is located at $z_M = 2.3r_0$, the cell here is shorter, with $z_M = 1.85r_0$. The Mach disk is also thicker than in the free jet. An annular oblique shock is visible around the Mach disk, as in Jetfree. The temporal evolution of the jet shows a strong axial motion of the Mach disk, as experimentally observed by Risborg & Soria.[9] Moreover, the periodic motion of the Mach disk is synchronized with the strong spherical sound waves visible in the pressure field. In figure 13(b), for JetL5, the first cell of the shock-cell structure is similar to that in Jetfree. A Mach disk forms upstream from the plate, at $z = 4.25r_0$, in the second cell. In the pressure field, sound waves seem to propagate from the region of the impact. In figure 13(c), for JetL7, the two first cells of the shock-cell structure resemble those in Jetfree. Two acoustic contributions are visible in the pressure field. First, wavefronts centered around the annular oblique shock of the first cell appear. They are due to the interactions between the oblique shock and the turbulence in the shear layers. A second acoustic contribution seems to come from the region of impact. Finally, in figure 13(d), for JetL9, a Mach disk forms upstream from the plate at $z = 7.7r_0$, in the third cell. The pressure field looks like the pressure field of JetL7.

IV.B. Mean flows

The mean velocity fields obtained in the (r, z) plane are presented in figure 14. A good agreement is found with the measurements of Henderson *et al.*[8] For JetL5 and JetL7, however, shock cells are slightly shorter in the simulation than in the experiment. For JetL4, in figure 14(a), the effects of the flat plate on the first shock cell mentioned previously are clearly visible. For JetL5 and JetL9, a second cell and a third cell, respectively, cannot fully form before the plate, and a Mach disk is generated close to the wall. On the contrary, for JetL7, in figure 14(c), the two first cells of the shock-cell structure appear to spread over the entire space between the nozzle and the plate, and no Mach disk is created upstream from the plate. Finally, for JetL4, JetL5 and JetL9, recirculation zones are found on each side of the jet near the plate, in agreement with the experiments of Henderson & Powell,[6] Krothapalli *et al.*[7] and Henderson *et al.*[8] These results are also in line with the observations of Kuo & Dowling[12] who noted the appearance of a recirculation zone when the distance between the Mach disk and the flat plate exceeds $1.2r_0$. This distance is indeed equal to $2.3r_0$, $1.35r_0$ and $1.6r_0$ for JetL4, JetL5 and JetL9.

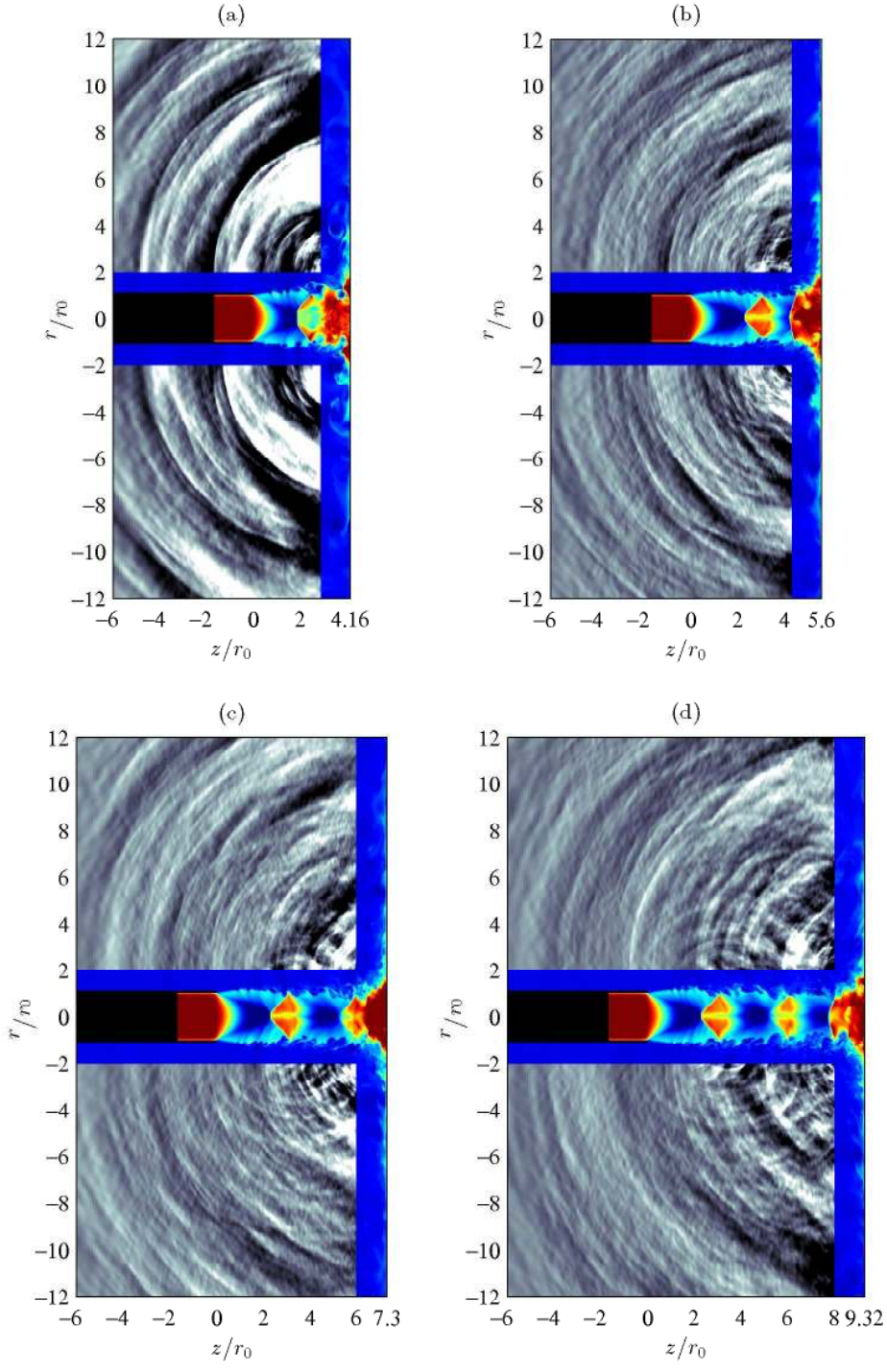

Figure 13. Snapshots in the (z, r) plane of the density in the jet and close to the flat plate, and of the fluctuating pressure for (a) JetL4, (b) JetL5, (c) JetL7 and (d) JetL9. The colour scale ranges from 1 to 3 kg.m^{-3} for the density and from −2000 to 2000 Pa for the pressure.

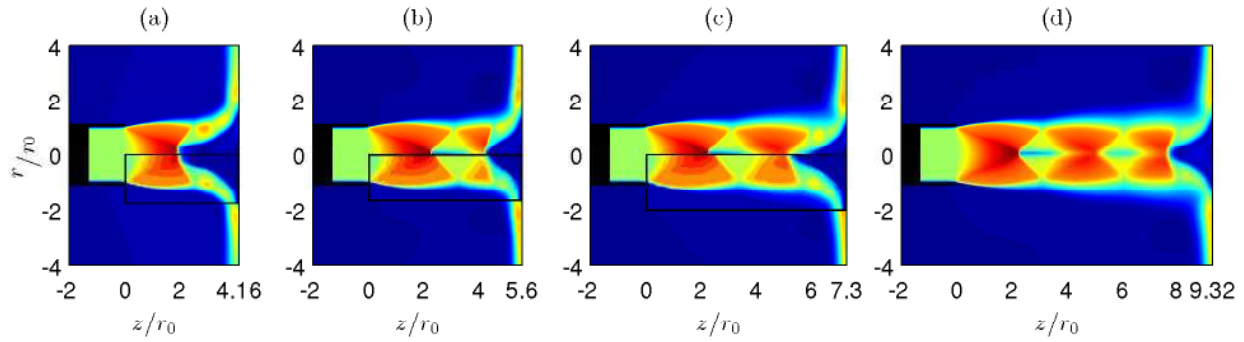

Figure 14. Mean velocity fields in the (z, r) plane for (a) JetL4, (b) JetL5, (c) JetL7 and (d) JetL9. The colour scale ranges from 0 to 500 m.s^{-1}. The experimental results of Henderson *et al.*[8] are represented in the black rectangles.

IV.C. Convection velocity

The convection velocity u_c of the large-scale structures in the jet shear layers has been estimated. It has been calculated at the center of the shear layer, whose position is given by the maximum of the root mean square of velocity fluctuations. The resulting path for JetL9 is for example displayed in figure 15. Along this path, axial velocity cross-correlations are computed to obtain the convection velocity. The results are shown in figure 16(a) for the free jet and the impinging jets.

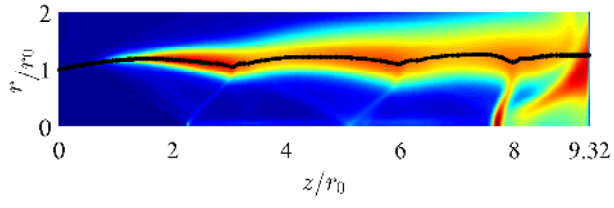

Figure 15. Root mean square values of velocity fluctuations for JetL9. The color scale ranges from 0 to 100 m.s^{-1}. The black line shows the position of the maximum values.

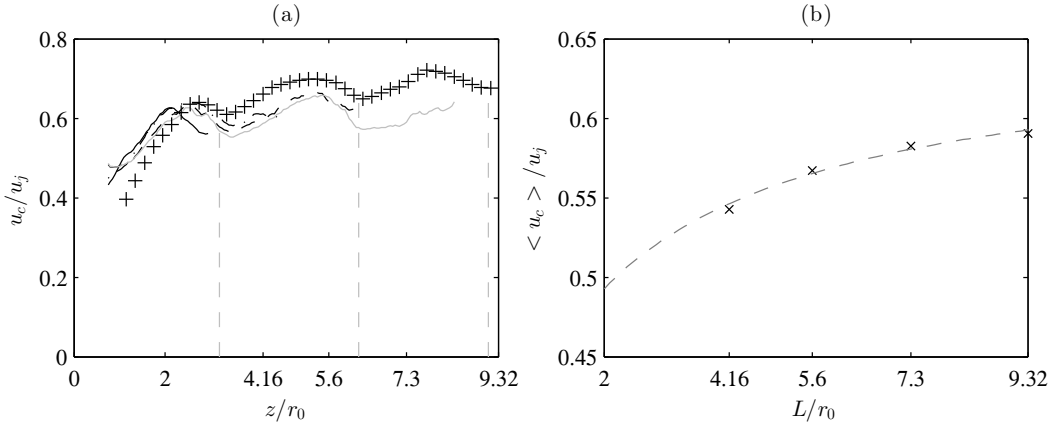

Figure 16. (a) Convection velocity of the large scale structures in the shear layers for —— JetL4, —·— JetL5, — — — JetL7, —— JetL9 and + + + Jetfree. The dashed vertical grey lines correspond to the end of the cells in the shock-cell structure of the free jet. (b) Mean convection velocity between the nozzle and the plate for: × the four impinging jets and — — — the expression 8.

The convection velocity in the shear layers is not constant but varies according to the shock-cell structure. In the first cell, the convection velocity increases between the nozzle lips and the position of the Mach disk, as the velocity inside the jet grows, and then decreases down to the end of the cell, following the velocity reduction in the jet downstream of a Mach disk or an oblique shock. Similar variations can be seen for all cells. They are consistent with the experimental results obtained by Westley & Woolley[37] and by André

et al.[31] for imperfectly expanded round jets. The modification of the first shock cell in JetL4 described earlier is also visible in figure 16, with a maximum of the convection velocity reached around $z_M = 1.85r_0$ for JetL4 but around $z_M = 2.3r_0$ for the other jets. Moreover, for Jetfree, the convection velocity tends to a value around $u_c = 0.65u_j$ in the downstream direction, which is in good agreement with the experimental observations of Harper-Bourne & Fisher,[35] who found $u_c = 0.70u_j$ using a crossed-beam Schlieren technique.

Given the variations of the convection velocity in figure 16, it does not appear relevant to use the same convection velocity between the lip and the plate for all nozzle-to-plate distances, as was the case in the model of Ho & Nosseir[3] and Nosseir & Ho[4] to predict the frequencies of the feedback mechanism. Indeed, the average convection velocity between the nozzle and the flat plate for the four impinging jets, displayed in figure 16(b), varies from $0.54u_j$ for JetL4 up to $0.59u_j$ for JetL9. It can be approximated by the average convection velocity

$$< u_c > (L) = 0.65u_j - (0.65u_j - 0.5u_e)\frac{1}{1 + L/D_j} \tag{8}$$

which is represented in figure figure 16(b) for a nozzle-to-plate distance ranging from $L = 2r_0$ to $L = 10r_0$. Expression (8) tends to $0.65u_j$ for large distances L, in agreement with the result of Jetfree, and tends to $0.5u_e$ near the nozzle, as expected.

IV.D. Pressure spectra

The sound pressure levels obtained at $r = 2r_0$ and $z = 0$ are plotted in figure 17 as a function of the Strouhal numbers $St_D = fD/u_e$. The Strouhal number of the tones whose levels are 5 dB higher than the broadband noise are given in table 3.

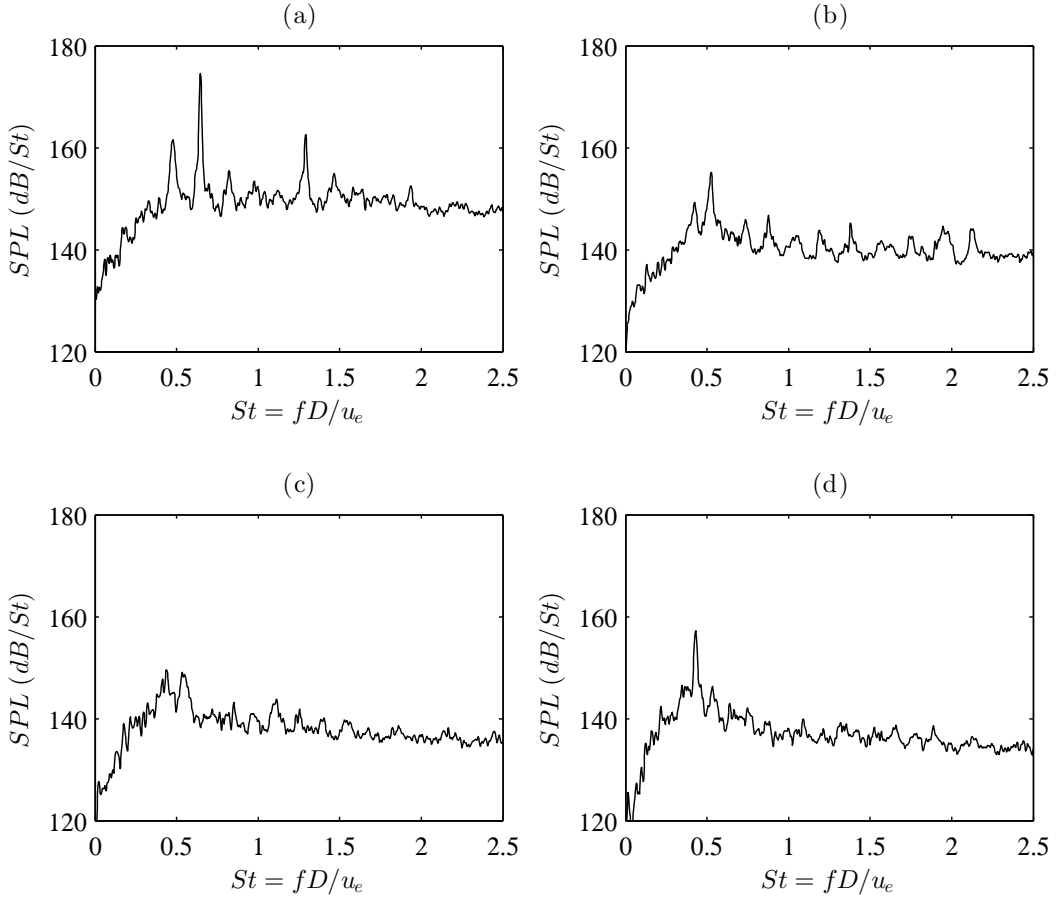

Figure 17. Sound pressure levels (SPL) at $r = 2r_0$ and $z = 0$ as a function of the Strouhal number for (a) JetL4, (b) JetL5, (c) JetL7 and (d) JetL9.

For JetL4, in figure 17(a), three tones emerge at Strouhal numbers $St_1 = 0.475$, $St_2 = 0.645$ and $St_3 = 1.29$, with $St_3 = 2St_2$. The dominant tone, at $St_2 = 0.645$, emerges 20 dB above the broadband noise. It corresponds to the axially pulsing motion of the Mach disk noted in figure 13(a). These results agree with the experiments of Henderson *et al.*,[8] who obtained a fundamental tone frequency at $St_D = 0.67$, and with the simulation of Dauptain *et al.*,[15] who also found an axially pulsing mode for a similar impinging jet. For JetL5, in figure 17(b), several tone frequencies are observed at Strouhal numbers between 0.4 and 2. The fundamental tone frequency, emerging around 10 dB above the broadband noise, is visible at $St_2 = 0.525$. This value is consistent with the experimental findings of Henderson *et al.*,[8] who measured a fundamental tone at $St_D = 0.52$ for the same jet. For JetL7, in figure 17(c), two tone frequencies emerge around 6 dB above the broadband noise. The dominant tone obtained at $St_1 = 0.44$ compares well with the fundamental tone frequency observed[8] experimentally at $St_D = 0.42$. Finally, for JetL9, in figure 17(d), the fundamental tone frequency corresponds to a Strouhal number of $St_1 = 0.43$.

	St_1	St_2	St_3
JetL4	0.475	**0.645**	1.29
JetL5	**0.525**	-	-
JetL7	**0.44**	0.54	-
JetL9	**0.43**	-	-

Table 3. Strouhal numbers emerging in the spectra of figure 17. The Strouhal number of the dominant tone in each case appears in bold.

For JetL4, JetL7 and JetL9, a Mach disk forms just upstream of the flat plate, and strong tones are obtained. On the contrary, for JetL7, the emerging tones are weak. These results are consistent with the experimental results of Henderson & Powell[6] who noted that the feedback mechanism establishes when there is a Mach disk upstream from the plate and ceases when there is a conical shock wave instead.

IV.E. Tone frequencies

In order to explain the tone frequencies measured for supersonic impinging jets, Powell[1] suggested that a feedback mechanism establishes between the nozzle lips and the flat plate. This mechanism consists of two steps. First, in the jet shear layers, a coherent structure is convected downstream from the nozzle to the plate. The structure impinges on the plate, and generates an acoustic wave propagating upstream towards the nozzle. This wave is then reflected by the nozzle lip, which excites the shear layer, and leads to the formation of a new coherent structure. The fundamental period T_0 of this feedback loop corresponds to the sum of the time necessary for a coherent structure to travel downstream from the nozzle to the plate and the time of propagation of an acoustic wave from the plate to the nozzle, yielding

$$T_0 = \int_0^L \frac{1}{u_c(z)} dz + \frac{L}{c_0} = \frac{N+p}{f} \tag{9}$$

where $u_c(z)$ is the convection velocity in the shear layers, c_0 is the speed of sound, p is a phase lag at the nozzle exit, and the mode number N indicates the number of time the feedback mechanism occurs during the fundamental period T_0.

Powell[1] argued that the phase lag p is not necessarily zero because the reflection of the acoustic wave on the nozzle lips and the creation of a coherent structure in the shear layer are not simultaneous phenomena. In experiments, Krothapalli *et al.*[7] found for instance $p = 0$ for subsonic round jets and $p = -0.4$ for supersonic round jets. Later, Ho & Nosseir[3] and Nosseir & Ho[4] investigated the near field pressure of jets impinging on a flat plate normally, and proposed an empirical model for predicting the frequencies of the feedback mechanism, this model writes

$$\frac{N}{f} = \frac{L}{< u_c >} + \frac{L}{c_0} \tag{10}$$

where $< u_c >$ is the mean convection velocity of the large-scale structures in the shear layers between the nozzle and the plate. Here, the phase lag p is considered null.

The Strouhal numbers of the dominant tone frequencies collected in table 3 for the present jets are shown in figure 18 as a function of the nozzle-to-plate distance L/r_0. The experimental tone frequencies obtained

by Henderson[29] for underexpanded supersonic round jets characterized by Nozzle Pressure Ratios of 3.80, 4.03, 4.15 and 4.50 as well as the tone frequencies predicted by the expression (10) are also displayed. In the latter case, the mean convection velocity $< u_c > (L)$ is given by the proposed expression (8).

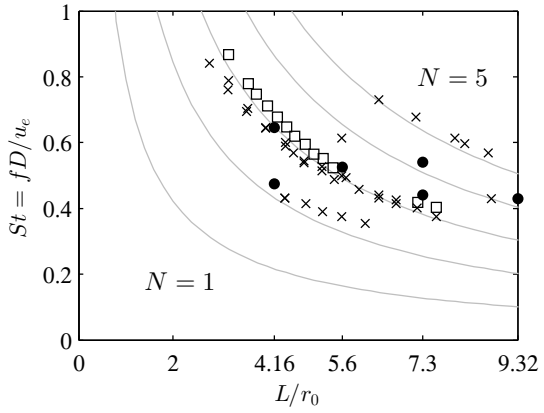

Figure 18. Strouhal number of the tone frequencies obtained: • for the present impinging jets, □ experimentally by Henderson *et al.*[8] for $NPR = 4.03$ and × experimentally by Henderson[29] for $NPR = 3.80$, 4.15 and 4.50. The grey lines show the values predicted by the expression (10).

A good agreement is found between the simulation and the experimental data. Moreover, the tone frequencies seem to be well predicted by the model of Ho & Nosseir[3] and Nosseir & Ho[4] using expression (8). The dominant tone frequencies in JetL4 are associated with the second and third modes of the model. As the nozzle-to-plate increases, a switch from the second mode to the third mode is obtained for JetL5, and a second switch from the third mode to the fourth mode happens in JetL7 and in JetL9. The dominant tone frequencies thus remain between $St = 0.43$ and $St_D = 0.645$ for the present jets. Such a staging behaviour of the dominant tone frequency as the nozzle-to-plate distance varies, is typical of feedback mechanisms, see the experiments of Wagner[2] and Henderson,[29] among others.

IV.F. Fourier decomposition of the pressure field

The near pressure fields of the impinging jets have been recorded every 50^{th} time step and decomposed using a Fast Fourier Transform the same way as the pressure field of Jetfree. The amplitude fields thus obtained for the dominant tone frequencies are shown in the top views of figure 19, and the phase fields are displayed in the bottom views.

As there is no phase shift on both sides of the jet axis in figure 19(e), the fundamental tone frequency of JetL4 is associated with a varicose mode. This result is consistent with the axially pulsing motion of the Mach disk reported previously and with the experiments of Henderson *et al.*[8] who obtained symmetrical jet oscillations for a similar impinging jet. On the contrary, a 180 degree phase shift is visible with respect to the jet axis in the phase fields of the dominant tone frequencies of JetL5, JetL7 and JetL9, indicating a sinuous or helical mode. More precisely, based on a Fourier decomposition of the fluctuating pressure on 32 sensors regularly spaced in the azimuthal direction at $z = 0$ and $r = 2r_0$, the mode is helical for the three cases.

Information on the sound sources are also provided by the amplitude and phase fields of figure 19. For a better description, let α be the angle at the impingement region between the upstream direction and the waves propagating from the flat plate, as illustrated in figure 19(a). For the dominant tone frequency of JetL4, in figures 19(a) and 19(e), two acoustic contributions are revealed. Indeed, two regions of constructive interferences appear in the amplitude field. The first acoustic contribution can be seen in the shear layers of the jet and in the near field on each side of the nozzle, for $0 \leq \alpha \leq 20$ degrees. This contribution corresponds to the upstream propagating acoustic waves which close the feedback mechanism. The second contribution is visible for $40 \leq \alpha \leq 70$ degrees and seems to be generated from a point located on the plate at $r \simeq 3r_0$. This position coincides with an intense spot in the amplitude field. Destructive interferences can be seen for $\alpha \simeq 30$ degrees between the two acoustic contributions in figure 19(e) with a strong reduction of the amplitude in this direction. The far-field noise in the sideline directions is thus mainly due to the second contribution and the localisation of the intense spot in the amplitude field on the plate at $r \simeq 3r_0$

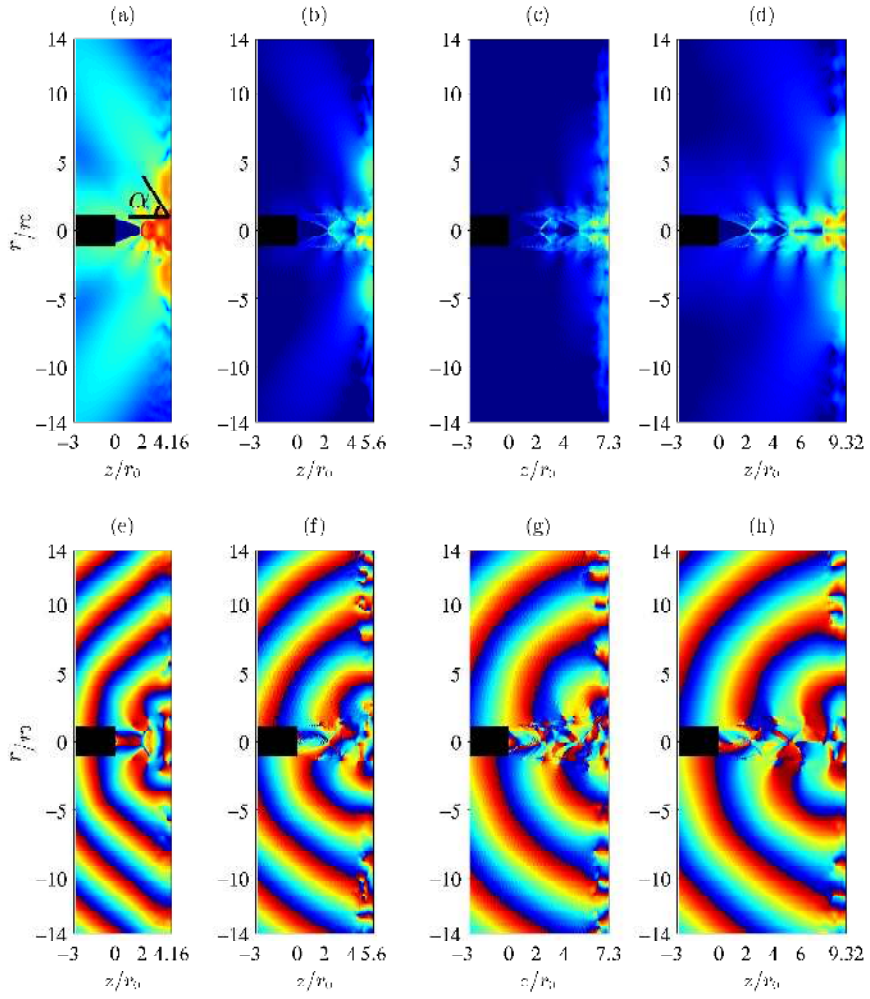

Figure 19. Amplitude (top) and phase (bottom) fields obtained for the dominant tone frequency in (a) and (e) JetL4 ($St_D = 0.645$), (b) and (f) JetL5 ($St_D = 0.525$) (c) and (g) JetL7 ($St_D = 0.44$) and (d) and (h) JetL9 ($St_D = 0.43$).

in figure 19(a) corresponds to the acoustic source found experimentally by Henderson *et al.*,[8] for a similar impinging jet, on an annular region on the plate, at $r = 2.6r_0$. For the dominant tone frequencies of JetL5 and JetL9, two acoustic contributions can similarly be noted. The second contribution seems to come from a point located on the plate at $r \simeq 4r_0$. Finally, for the dominant tone frequency of JetL7, there is no clear destructive interferences. Only one acoustic contribution appears to propagate from the region of impact.

V. Conclusion

In this paper the flow and near pressure fields of a free jet and four impinging underexpanded jets have been presented. They have a fully expanded Mach number of $\mathcal{M}_j = 1.56$, a Reynolds number of $Re_j = 5\times10^4$ and an exit Mach number of $\mathcal{M}_e = 1$. The free jet is first investigated. Flow snapshots of vorticity, density and pressure as well as mean velocity fields are shown. The results, including the shock-cell structure, are consistent with experimental data, empirical and theoretical models. A tone frequency associated with screech noise is obtained in the near pressure field of the jet. Its frequency and helical nature agree well with the model of Panda[38] describing the formation of an hydrodynamic-acoustic standing wave and with the measurements of Powell *et al.*[39]

The four impinging jets are then studied. Flow snapshots and the mean fields of the jets are presented and compared with experimental data and with the results of the free jet. The convection velocity in the shear layers of the jets is evaluated. An expression yielding the mean convection velocity between the nozzle and the flat plate, for nozzle-to-plate distances L ranging from $2r_0$ to $10r_0$, is then proposed. The near

pressure fields reveal several tone frequencies. A staging phenomenon of the main tone frequency with the nozzle-to-plate distance is found, which is typical of an aeroacoustic feedback mechanism occurring between the nozzle lip and the flat plate. The different models existing for the mechanism are presented and the model of Ho & Nosseir[3] and Nosseir & Ho[4] is applied using the expression (8) giving the average convection velocity $< u_c > (L)$. A very good agreement is found for the tone frequencies obtained. Finally, the nature of the dominant modes is identified. The results are consistent with experimental and numerical results. Notably, the strength of the feedback mechanism appears to be correlated with the formation of a Mach disk upstream of the plate, as noted by Henderson & Powell.[6]

In further work, the underlying physics of the feedback mechanism will be explored. This will be done by extracting the most energetic modes by proper orthogonal decomposition and by using dynamic mode decomposition. The effect of the Mach disk position and motion on the feedback mechanism will then be studied.

Acknowledgments

This work was performed using HPC resources of P2CHPD (Pôle de Calcul Hautes Performances Dédiés) and IDRIS (Institut du Développement et des Ressources en Informatique Scientifique) under the allocation 2014-2a0204 made by GENCI (Grand Equipement National de Calcul Intensif). This work was performed within the framework of the Labex CeLyA of Université de Lyon, within the program "Investissements d'Avenir" (ANR-10-LABX-0060/ ANR-11-IDEX-0007) operated by the French National Research Agency (ANR).

References

[1]Powell, A., "On edge tones and associated phenomena", *Acta Acust. United Ac.*, Vol. 3, 1953, pp. 233-243.

[2]Wagner, F.R., "The sound and flow field of an axially symmetric free jet upon impact on a wall", *NASA*, 1971, NASA TT F-13942.

[3]Ho, C.M. and Nosseir, N.S., "Dynamics of an impinging jet. Part 1. The feedback phenomenon", *J. Fluid Mech.*, Vol. 105, 1981, pp. 119-142.

[4]Nosseir, N.S. and Ho, C.M., "Dynamics of an impinging jet. Part 2. The noise generation", *J. Fluid Mech.*, Vol. 116, 1982, pp. 379-391.

[5]Tam, C.K.W. and Ahuja, K.K., "Theoretical model of discrete tone generation by impinging jets", *J. Fluid Mech.*, Vol. 214, 1990, pp. 67-87.

[6]Henderson, B. and Powell, A., "Experiments concerning tones produced by an axisymmetric choked jet impinging on flat plates", *J. Sound Vib.*, Vol. 168, No. 2, 1993, pp. 307-326.

[7]Krothapalli, A., Rajkuperan, E., Alvi, F. and Lourenco, L., "Flow field and noise characteristics of a supersonic impinging jet", *J. Fluid Mech.*, Vol. 392, 1999, pp. 155-181.

[8]Henderson, B., Bridges, J. and Wernet, M., "An experimental study of the oscillatory flow structure of tone-producing supersonic impinging jets", *J. Fluid Mech.*, Vol. 542, 2005, pp. 115-126.

[9]Risborg, A. and Soria, J., "High-speed optical measurements of an underexpanded supersonic jet impinging on an inclined plate", *28th International Congress on High-Speed Imaging and Photonics*, Vol. 7126, 2009.

[10]Buchmann, N.A., Mitchell, D.M., Ingvorsen, K.M., Honnery, D.R. and Soria, J., "High spatial resolution imaging of a supersonic underexpanded jet impinging on a flat plate", *Sixth Australian Conference on Laser Diagnostics in Fluid Mechanics and Combustion*, Vol. 116, 2011

[11]Mitchell, D.M., Honnery, D.R. and Soria, J., "The visualization of the acoustic feedback loop in impinging underexpanded supersonic jet flows using ultra-high frame rate schlieren", *J. of visualization*, Vol. 15, No. 4, 2012, pp. 333-341.

[12]Kuo, C.Y. and Dowling, A.P., 'Oscillations of a moderately underexpanded choked jet impinging upon a flat plate", *J. Fluid Mech.*, Vol. 315, No. 4, 1996, pp. 267-291.

[13]Powell, A., "The sound-producing oscillations of round underexpanded jets impinging on normal plates", *J. Acoust. Soc. Am.*, Vol. 83, No. 2, 1988, pp. 515-533.

[14]Dauptain, A., Cuenot, B. and Gicquel, L.Y.M., "Large eddy simulation of stable supersonic jet impinging on flat plate", *AIAA J.*, Vol. 48, No. 10, 2010, pp. 2325-2338.

[15]Dauptain, A., Gicquel, L.Y.M. and Moreau, S., "Large Eddy Simulation of Supersonic Impinging Jets", *AIAA J.*, Vol. 50, No. 7, 2012, pp. 1560-1574.

[16]Bogey, C. and Bailly, C., "A family of low dispersive and low dissipative explicit schemes for flow and noise computations", *J. Comput. Phys.*, Vol. 194, No. 1, 2004, pp. 194-214.

[17]Berland, J., Bogey, C., Marsden, O. and Bailly, C., "High-order, low dispersive and low dissipative explicit schemes for multiple-scale and boundary problems", *J. Comput. Phys.*, Vol. 224, No. 2, 2007, pp. 637-662.

[18]Bogey, C. and Bailly, C., "Large eddy simulations of transitional round jets: influence of the Reynolds number on flow development and energy dissipation", *Phys. Fluids*, Vol. 18, No. 065101, 2006, pp. 1-14.

[19]Bogey, C. and Bailly, C., "Turbulence and energy budget in a self-preserving round jet: direct evaluation using large eddy simulation", *J. Fluid Mech.*, Vol. 627, 2009, pp. 129-160.

[20]Tam, C.K.W. and Dong, Z., "Wall boundary conditions for high-order finite-difference schemes in computational aeroacoustics", *Theor. Comput. Fluid Dyn*, Vol. 6, 1994, pp. 303-322

[21]Bogey, C., Marsden, O. and Bailly, C., "Large-eddy simulation of the flow and acoustic fields of a Reynolds number 10^5 subsonic jet with tripped exit boundary layers", *Phys. Fluids*, Vol. 23, 2011, pp. 035104.

[22]Bogey, C., Marsden, O. and Bailly, C., "Influence of initial turbulence level on the flow and sound fields of a subsonic jet at a diameter-based Reynolds number of 10^5", *J. Fluid Mech.*, Vol. 701, 2012, pp. 352-385.

[23]Bogey, C., de Cacqueray, N. and Bailly, C., "A shock-capturing methodology based on adaptative spatial filtering for high-order non-linear computations", *J. Comput. Phys.*, Vol. 228, 2009, pp. 1447-1465.

[24]de Cacqueray, N., Bogey, C. and Bailly, C., "Investigation of a High-Mach-Number Overexpanded Jet Using Large-Eddy Simulation", *AIAA J.*, Vol. 49, No. 10, 2011, pp.2171-2182.

[25]Mohseni, K. and Colonius, T., "Numerical treatment of polar coordinate singularities", *J. Comput. Phys.*, Vol. 157, No. 2, 2000, pp. 787-795.

[26]Bogey, C., de Cacqueray, N. and Bailly, C., "Finite differences for coarse azimuthal discretization and for reduction of effective resolution near origin of cylindrical flow equations", *J. Comput. Phys.*, Vol. 230, No. 4, 2011, pp. 1134-1146.

[27]Lau, J.C., Morris, P.J. and Fisher, M.J., "Measurements in subsonic and supersonic free jets using a laser velocimeter", *J. Fluid Mech.*, Vol. 93, 1979, pp. 1-27.

[28]Tam, C.K.W., Jackson, J.A. and Seiner, J.M., "A multiple-scales model of the shock-cell structure of imperfectly expanded supersonic jets", *J. Fluid Mech.*, Vol. 153, 1985, pp. 123-149.

[29]Henderson, B., "The connection between sound production and jet structure of the supersonic impinging jet", *J. Acoust. Soc. Am.*, Vol. 111, No. 2, 2002, pp. 735-747.

[30]Addy, A.L., "Effects of axisymmetric sonic nozzle geometry on Mach disk characteristics", *AIAA J.*, Vol. 19, No. 1, 1981, pp. 121-122.

[31]André, B., Castelain, T. and Bailly, C., "Investigation of the mixing layer of underexpanded supersonic jets by particle image velocimetry", *IJHFF*, Vol. 50, 2014, pp. 188-200.

[32]Prandtl, L., "Über die stationären Wellen in einem Gasstrahl", 1904.

[33]Tam, C.K.W. and Tanna, H.K., "Shock associated noise of supersonic jets from convergent-divergent nozzles", *J. Sound Vib.*, Vol. 81, No. 3, 1982, pp. 337-358.

[34]Pack, D.C., "A note on Prandtl's formula for the wave-length of a supersonic gas jet", *The Quarterly Journal of Mechanics and Applied Mathematics*, Vol. 3, No. 2, 1950, pp. 173-181.

[35]Harper-Bourne, M. and Fisher, M.J., "The noise from shock in supersonic jets", *AGARD Conference on Noise Mechanisms*, Vol. AGARD-CP-131, 1973, pp. 1-11.

[36]Seiner, J.M. and Norum, T.D., "Aerodynamic aspects of shock containing jet plumes", *AIAA 6th Aeroacoustics conference*, 1980, AIAA Paper 80-0965.

[37]Westley, R. and Woolley, J.H., "The near field sound pressures of a choked jet during a screech cycle", *AGARD C.P.*, Vol. 42, 1969, pp. 23-1-23-13.

[38]Panda, J., Raman, G. and Zaman, K.B.M.Q., "Underexpanded screeching jets from circular, rectangular and elliptic nozzles", *3th AIAA/CEAS Aeroacoustics conference*, 1997, AIAA Paper 97-1623

[39]Powell, A., Umeda, Y. and Ishii, R., "Observations of the oscillation modes of choked circular jets", *J. Acoust. Soc. Am.*, Vol. 92, No. 5, 1992, pp. 2823-2836.

[40]Arnette, S.A., Samimy, M. and Elliott, G.S., "On streamwise vortices in high Reynolds number supersonic axisymmetric jets", *Phys. Fluids*, Vol. 5, No. 1, 1993, pp. 187-202.